Defense Technical Information Center
Compilation Part Notice

ADP012062

TITLE: Accuracy of Currents Produced by the Locally-Corrected Nystrom Method and the Method of Moments when used with Higher-Order Representations

DISTRIBUTION: Approved for public release, distribution unlimited

This paper is part of the following report:

TITLE: Applied Computational Electromagnetics Society Journal. Volume 17, Number 1

To order the complete compilation report, use: ADA399939

The component part is provided here to allow users access to individually authored sections of proceedings, annals, symposia, etc. However, the component should be considered within the context of the overall compilation report and not as a stand-alone technical report.

The following component part numbers comprise the compilation report:
ADP012055 thru ADP012066

Accuracy of currents produced by the Locally-Corrected Nyström Method and the Method of Moments when used with higher-order representations

Andrew F. Peterson
School of Electrical and Computer Engineering
Georgia Institute of Technology
Atlanta, GA 30332-0250
peterson@ee.gatech.edu

Abstract: The locally-corrected Nyström method is described, and the accuracy of the currents produced by it and the method of moments are compared. Results suggest that when the underlying representation has the same degree, the methods are comparable in accuracy. Additional results are presented to illustrate the Nyström approach, and advantages and disadvantages of the method are reported.

Introduction

The method of moments (MoM) for solving integral equations [1] has been widely used for more than three decades, and is generally well-accepted throughout the electromagnetics community. The process involves representing an unknown quantity with a known basis, and weighting the moments of the equation to be solved with suitable testing functions to form a linear system. The method is well-suited for treating equations with singular kernels, since it incorporates integrals over testing functions which ultimately reduce the order of singularities.

The Nyström method for the solution of integral equations was proposed in 1930 [2]. The essence of the approach is that the integral operator is replaced with a suitable quadrature rule. The integral equation is enforced at nodes (sample points) of the rule, and leads to a linear system of equations for the samples of the unknown function at the node points. The drawback of the classical Nyström method is that it cannot be used directly for integral equations with singular

kernels [3]. Only recently has the method been extended to treat the singular integral equations arising in electromagnetic radiation and scattering problems [4-5]. The extended method is known as the locally-corrected Nyström (LCN) method. Reference [4] provides an in-depth discussion of the LCN method for application to two- and three-dimensional electromagnetic scattering problems. Reported advantages of the LCN method are that it is well-suited for higher-order implementation, offers reduced matrix fill costs, and is easily amenable to fast iterative solvers such as the fast multipole method.

Although references [4-5] provided a comparison of data for LCN scattering cross section calculations, they did not specifically report the accuracy of the currents (or the internal fields in the case of [5]). In this paper, the accuracy of the currents produced by the method of moments and the locally-corrected Nyström method will be compared for the TE electric-field integral equation (EFIE) for conducting cylinders. The ease of use and relative efficiency will be reported, as will differences in philosophy between the methods and differences in their implementation.

The Method of Moments Implementation

Consider the MoM approach for solving the TE EFIE for two-dimensional scattering from perfectly conducting cylinders. The operator in this case is an integro-differential operator with two derivatives that can be distributed between

the current density, the Green's function, or the testing functions. This type of operator is also referred to as a *hypersingular* integral operator [4]. Since the TE EFIE operator involves derivatives, it is generally thought that a key requirement of the MoM implementation is that the cell-to-cell continuity of the current be maintained by the basis functions, to avoid fictitious line charge densities associated with jump discontinuities in the current. A widespread implementation uses pulse (piecewise-constant) testing functions to absorb one of the derivatives and piecewise-linear basis functions to provide a minimum degree of differentiability while preserving cell-to-cell continuity [6].

For purposes of this study, an MoM implementation was developed for the TE EFIE using pulse testing functions with basis functions that can range in degree from piecewise linear to piecewise cubic. The cylinder contour of interest is divided into cells, each with parabolic shape to better represent curved surfaces. The basis functions are Lagrangian polynomials that span each cell and have evenly-spaced interpolation points throughout each cell. Continuity between cells is maintained by associating the functions interpolating at the boundary between adjacent cells with the same coefficient. Matrix entries are computed with the aid of Gaussian quadrature rules that incorporate the logarithmic singularity of the two-dimensional free-space Green's function when necessary [7].

The LCN Implementation

The TE EFIE incorporates the scatttered field at location t obtained from the operator

$$-\hat{t} \cdot \bar{E}^s = j\frac{\eta}{k} \int K(t,t')\, J(t')\, dt' \qquad (1)$$

where the unit vector is tangential to the contour of the cylinder at t, k is the wavenumber, η is the medium impedance, J is the current density phasor, and

$$K(t,t') = \{k^2\cos(\Omega_o - \Omega_s)$$
$$+ \cos\Omega_o \cos\Omega_s \frac{\partial^2}{\partial x^2}$$
$$+ \sin(\Omega_o + \Omega_s) \frac{\partial^2}{\partial x \partial y}$$
$$+ \sin\Omega_o \sin\Omega_s \frac{\partial^2}{\partial y^2}\} \frac{1}{4j} H_0^{(2)}(kR) \qquad (2)$$

where Ω_o and Ω_s denote the angles between the x-axis and the contour tangent vectors at the observer and source points, $H_0^{(2)}$ denotes the Hankel function, and

$$R = \sqrt{[x(t)-x(t')]^2 + [y(t)-y(t')]^2} \qquad (3)$$

The Nyström approach involves replacing the integral operator in (1) by a suitable quadrature rule:

$$-\hat{t}(t) \cdot \bar{E}^s = j\frac{\eta}{k} \sum_p w_p J(t_p) K(t,t_p) \qquad (4)$$

where $\{w_p, t_p\}$ denote the weights and sample points of the rule. If K is nonsingular, (4) can be evaluated at any location t. Under these conditions the EFIE

$$\hat{t}(t) \cdot \bar{E}^{inc} = -\hat{t}(t) \cdot \bar{E}^s \qquad (5)$$

may be enforced at each of the sample points t = t_p to obtain a linear system in terms of the samples of the current density as the primary unknown. (This is the classical Nyström method.) The TE EFIE kernel in (2) exhibits a strong singularity, however, and the rule in (4) cannot be used when R→0 since the result is infinite. In that case, a "local correction" to (4) is used, as proposed by the authors of [4].

The LCN discretization process is as follows. The cylinder contour is divided into cells, and a quadrature rule of a certain order is defined for each cell. (In the present study the quadrature order was the same in all cells.) For widely-spaced cells, the classical Nyström approach of equation (4) is employed for the interactions. For

unknowns $\{J(t_n)\}$, the LCN matrix entry for an observer at point with global index t_m and a source at point with global index t_n is given by the integrand sample

$$j\frac{\eta}{k}\ w_n\ K(t_m,t_n) \qquad (6)$$

Since most of the matrix entries represent widely-spaced interactions, the vast majority of the matrix entries have the form of (6).

When the observer and source points occur within closely-spaced cells (in the same cell or adjacent cells, in the present study), however, a completely different procedure is employed. This alternative approach involves replacing the singular kernel K by a nonsingular kernel L so that the scattered field can be computed using a similar expression:

$$-\hat{t}(t)\cdot\bar{E}^s = j\frac{\eta}{k}\sum_p w_p\ J(t_p)\ L(t,t_p) \qquad (7)$$

The process requires the synthesis of the needed samples of L so that the summation in (7) produces a correct overall result for the scattered electric field at each of the closely-spaced observation points.

A relatively small number of samples of L are required. These are obtained by selecting a set of "basis" functions $\{B_n(t)\}$ representing sources and enforcing the relatively small system of equations

$$j\frac{\eta}{k}\sum_p w_p\ B_n(t_p)\ L(t_m,t_p)$$

$$= -\frac{1}{T_m}\int_{t_m-T_m/2}^{t_m+T_m/2} \hat{t}(t)\cdot\bar{E}^s(B_n)\ dt \qquad (8)$$

where t_m is the observer location, t_p is the location within the source cell, and B_n represents a basis function for the current defined over the source cell. (The source and observer cells may coincide.) The expression on the right-hand side of (8) involves the scattered electric field at location t, produced by source function B_n, given by

$$\hat{t}(t)\cdot\bar{E}^s(B_n) = -j\frac{\eta}{k}\int K(t,t')\ B_n(t')\ dt' \qquad (9)$$

By this process, L is synthesized so that the summation in (7) yields the correct near fields of any source function J(t) that can be represented by the set $\{B_n\}$. The system in (8) must be solved for each observer location t_m.

As suggested by [4], an obvious choice for $\{B_n\}$ is the polynomial set underlying the quadrature rule (specifically, Legendre polynomials for Gauss-Legendre quadrature). We employ enough Legendre polynomials (constant, linear, etc.) to obtain a square linear system for (8). The basis functions are abruptly truncated at the cell edges, and the right hand side of (9) must incorporate the jump discontinuities in the basis functions at the source cell edges. To mitigate the effect of the singularity in the scattered field produced at each discontinuity, the scattered field is averaged over an interval of length T_m, centered at observation point t_m. The resulting expression is similar to an MoM matrix entry — and hence offers the convenience of using established procedures and legacy MoM software to obtain the right-hand side of (8). To maintain the linear independence of the equations in the case of P quadrature points per cell, and to mimic a direct sampling of the field so that the result in (7) smoothly merges with that of (4), we used an interval size 0.2/P of the cell extent. Experimentation showed little variation in the results as this interval size was perturbed.

The extent to which samples of L replace samples of K can vary; in this study (7) was used for all interactions between points in the same cell and in immediately adjacent cells. For an observer cell with P quadrature points, 3P solutions of P × P matrices are required to compute the entries of L. A more robust approach for small cells would monitor the extent to which samples of the integrand agree with those produced by the local correction procedure and adapt the size of the local correction region accordingly. (The singularity only arises for the real part of the kernel K; in [5] this is exploited by only correcting the real part of K. For simplicity, we

used the local corrections for both real and imaginary parts of K.)

In summary, interaction terms for "widely-spaced" source and observer points are obtained by sampling the integrand of the EFIE. Since these matrix entries are samples of the integrand in (1), and not an actual integral as the MoM matrix entries are, the LCN matrix fill time is usually substantially faster than the typical MoM fill time. Matrix entries for closely-spaced source and observer points are obtained by synthesizing a nonsingular integrand that, if sampled by the same quadrature rule, yield results for the integral equivalent to the actual field. As noted in [4], this process is similar to that proposed by Strain [8] to create quadrature rules for integrating singular functions. In the present implementation, the additional computational burden associated with solving the equations in (8) is only incurred for source and observer points in the same cell or immediately adjacent cells.

An interesting aspect of this Nyström approach is that no attempt is made to enforce cell-to-cell continuity. The representation for the current is implicitly defined by the quadrature rule (eg., a polynomial up to the degree that the rule can integrate) and is not constrained to be continuous across cell boundaries.

Representation Error

The MoM uses explicit basis functions to represent the current. The error in the current should follow the expected polynomial interpolation error for the particular basis functions. Consider a polynomial basis of degree p, where p=1 represents linear, p=2 represents quadratic, etc. For a problem with uniform cell size Δ, the expected interpolation error is of order $O(\Delta^{p+1})$. This error has been confirmed by example for integral equation formulations and the current density error appears to be independent of the testing function degree [9].

The underlying representation used by the LCN with Gauss-Legendre quadrature is also polynomial in nature, and an implementation using p+1 quadrature points per cell involves a polynomial representation of degree p. Thus, we again expect an error of $O(\Delta^{p+1})$ in the current produced by a (p+1)-point LCN implementation. For instance, the error produced by an MoM implementation with quadratic basis functions (p=2) should generally exhibit the same decay rate of $O(\Delta^3)$ as the cell sizes are reduced as an LCN implementation with 3 quadrature points per cell.

Results for circular cylinders

As an initial test case, we compare results from the MoM and LCN implementations for a circular cylinder of 6 λ circumference illuminated by a normally-incident plane wave. The angle $\phi = 180°$ represents the specular point on the cylinder in all cases. Figure 1 shows the error in the surface current density for the results of the MoM for linear, quadratic, and cubic basis functions when a 20-cell model is used to represent the cylinder contour. This error is defined as

$$\text{Absolute error} = |J_{ref} - J_{numerical}| \qquad (10)$$

and is determined at the quadrature nodes. Figure 2 shows LCN results for 2, 3, and 4 nodes per cell, for the same 20-cell model. For convenience, straight lines are used to connect samples of the error in both figures (the actual error may vary between nodes in a more complex manner). Both methods illustrate an improvement in accuracy as the order of the representation is increased. The reference solution was obtained to at least 5 decimal places using the eigenfunction series [10] and compared with the complex-valued surface current phasor at the interpolation points on the surface. The solution has a current magnitude that approaches 2.0 around the specular point and the errors in Figures 1 and 2 are the absolute errors on that same scale.
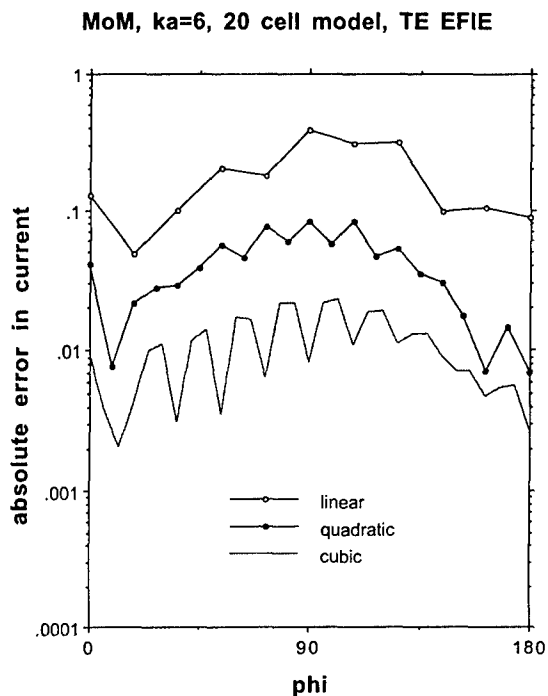
MoM, ka=6, 20 cell model, TE EFIE

Figure 1. The error in the MoM current for a circular cylinder, ka=6. Linear, quadratic, and cubic bases are used with a 20-parabolic-cell model.

In Figures 1 and 2, the linear-basis MoM (involving two overlapping basis functions per cell) exhibits current error that is generally comparable to that produced by the LCN implementation with 2 quadrature points per cell. The quadratic-basis MoM appears to produce an overall error level similar to the 3-point LCN result. These findings support the anticipated behavior of the current error as discussed above. However, the MoM basis functions impose cell-to-cell continuity, so one unknown coefficient is shared between cells. As a consequence, the MoM uses fewer unknowns to achieve a given level of accuracy. The unknown density in Figures 1 and 2 ranges from 3.3 unknowns/λ (20 unknowns distributed around 6 λ for the linear-basis MoM) to 13.3 unknowns/λ (80 unknowns distributed around 6 λ for the 4-point LCN). (The quadratic-basis MoM result used 40 unknowns; the 3-point LCN result with similar accuracy

required 60 unknowns.) Relative to the peak current magnitude of 2.0, the cubic basis MoM (10 unk/λ) and 4-point LCN (13.3 unk/λ) reduce the peak error in the current to 1 % or less.
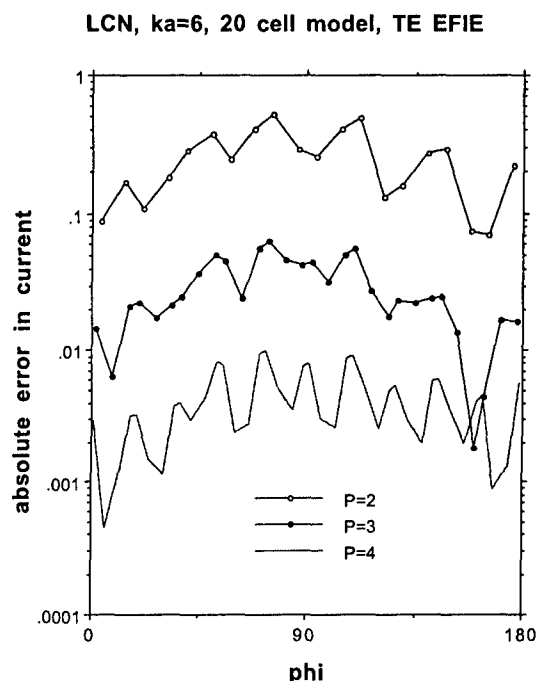
LCN, ka=6, 20 cell model, TE EFIE

Figure 2. The error in the LCN current for a circular cylinder, ka=6. A 20-parabolic-cell model is used with 2, 3, and 4 points per cell.

Figure 3 shows a plot of the error in the current for a circular cylinder with ka=11. The peak and average errors from the MoM with quadratic basis functions and LCN with 3 points per cell are compared, for cylinder models ranging from 10 cells to 100 cells. Both the peak and average error curves exhibit an $O(\Delta^3)$ behavior as the cell sizes are reduced, as predicted above. As in the previous example, the LCN requires more unknowns than the MoM for the same cell density.
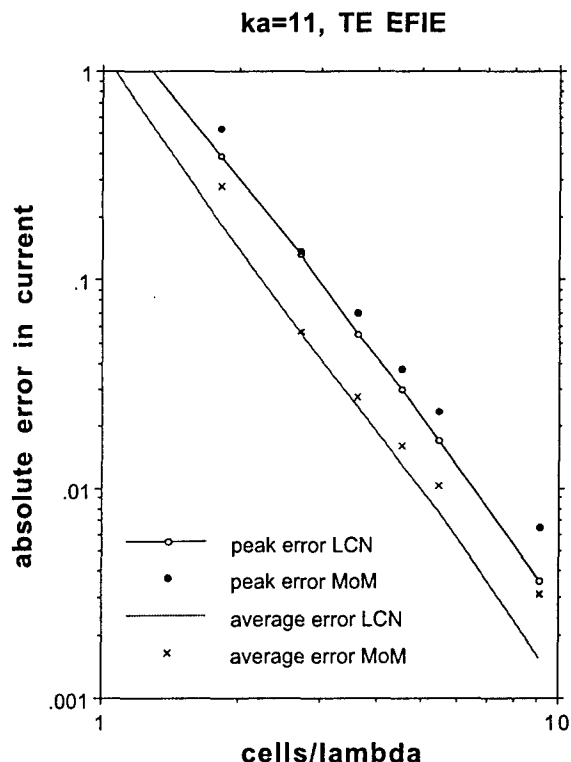
Figure 3. Comparison of the peak and average current error produced by the MoM with quadratic basis functions and the LCN with 3 points per cell, for a circular cylinder with ka=11. The current magnitude has a maximum value of approximately 2.0 at the specular point and the errors shown are the absolute errors on this scale. Averaging is performed around the circumference. The data appear to exhibit $O(\Delta^3)$ behavior.

From a comparison of Figures 1–3, and an investigation of other circular cylinder geometries, it appears that the overall accuracy between the MoM and the LCN is similar when the number of overlapping basis functions (MoM) equals the number of quadrature points (LCN). This result is in accordance with the expected $O(\Delta^{p+1})$ behavior. It also appears that because the MoM imposes cell-to-cell continuity, it uses fewer unknowns overall to achieve this accuracy.

Given the widespread notion that cell-to-cell continuity is a necessary condition for accurate solutions of the TE EFIE with the MoM, it is of

interest to examine the behavior of the surface current error within each cell. The LCN does not impose cell-to-cell continuity, and consequently one might expect to find larger errors near the cell edges. In fact, such behavior does seem to arise in the 4-point result in Figure 2. The opposite behavior is exhibited to some extent by the MoM result for cubic basis functions in Figure 1. However, the overall error of the 4-point LCN is no worse than the cubic basis MoM. From an examination of these data and other circular cylinder results (not shown), we find no evidence of a reduction in overall accuracy due to the non-continuous currents used by this LCN implementation. (This observation confirms that of the authors of [4].) This conclusion implies that a relaxation of continuity conditions might also be possible in MoM formulations.

Results for other cylinder shapes

As an additional comparison of the MoM and LCN for similar representation orders, Figure 4 shows the magnitude of the current density for a square cylinder with side dimension 5.2 λ. The cylinder is illuminated by a plane wave in an edge-on configuration. Results are shown for a 32-cell model (8 cells per face) with 4-point LCN and cubic-basis MoM implementations. A 3-point LCN result obtained from a 160-cell model is shown for comparison. (This reference solution was obtained from a combined-field formulation to ensure the absence of spurious internal resonance currents [11].)

Both the MoM result, involving a density of only 4.6 unknowns/λ, and the LCN result, involving 6.2 unknowns/λ, exhibit a noticeable but similar level of error compared with the reference solution. If the model is refined from 32 cells to 40 cells, the 4-point LCN (7.7 unk/λ) and cubic basis MoM (5.8 unk/λ) results for that model (not shown) are indistinguishable from the reference solution on the scale of Figure 4. These data support the previous findings that the MoM and LCN results for a given order of representation are similar.
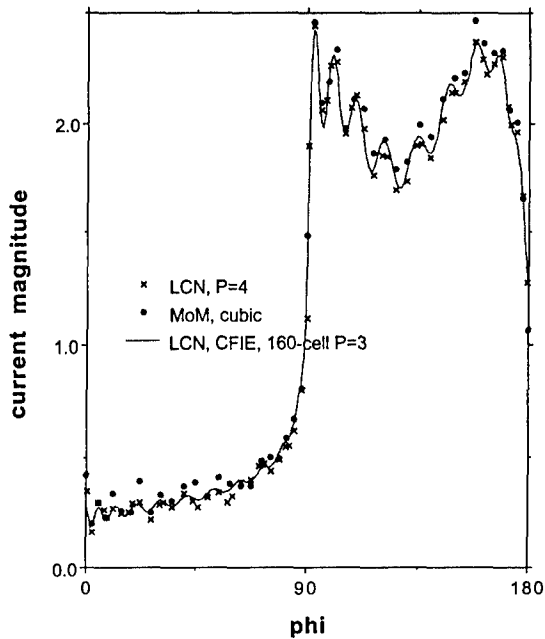
5.2 by 5.2 sq cyl, TE EFIE, 32-cell model

Figure 4. Comparison of the surface current produced by the MoM with cubic basis functions and the LCN with 4 points per cell, for a square cylinder with cross-sectional dimensions 5.2λ by 5.2λ, modeled with 32 cells. A reference solution obtained from a 160-cell model is shown for comparison.

As a final example, consider an elliptical cylinder with overall cross sectional dimensions 24λ by 6λ, illuminated along the narrow axis. This cylinder has a perimeter dimension of approximately 51λ. Figures 5, 6, and 7 show various LCN results obtained with 200, 100, and 70 cell models and 2–6 quadrature points per cell. This series of plots attempts to demonstrate the relative density of unknowns, for different degree representations, needed to obtain accurate solutions from the LCN approach, or equivalently, how the cell sizes used in the models may vary with changes in the number of quadrature points per cell.

Figure 5 shows results from 2 and 3-point LCN for a 200-cell model. The P=2 result (7.8 unk/λ) exhibits a noticeable error, while the P=3 result

(11.8 unk/λ) is in good agreement with the reference solution on the scale of the figure.
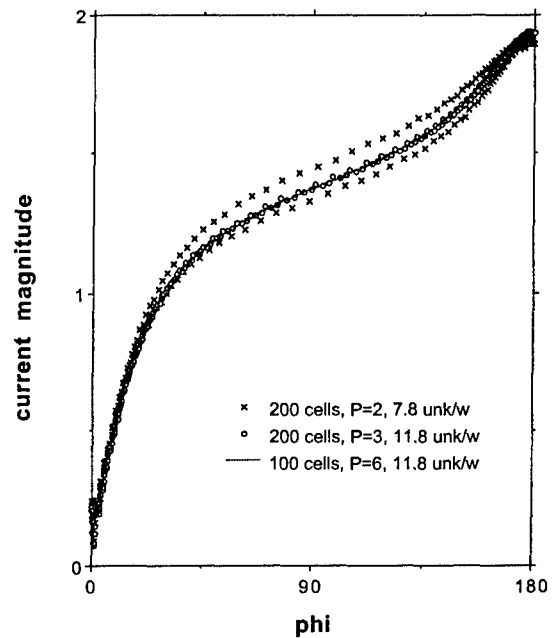
24 by 6 elliptical cylinder, TE CFIE

Figure 5. Results from the LCN method using a 200-cell model of an elliptical cylinder of dimensions 24λ by 6λ.

Figure 6 shows similar results from 3-point (5.9 unk/λ) and 4-point (7.8 unk/λ) LCN implementations obtained with a 100-cell model. The 3-point implementation exhibits considerable error, but the 4-point implementation appears correct on the scale of the figure (and at the same unknown density that produced a substantial error with the 2-point representation of Figure 5).

Figure 7 shows 5-point and 6-point LCN results obtained with a 70-cell model. The 5-point result, obtained with a density of 6.9 unknowns/λ, exhibits a slight error relative to the other curves. These figures suggest a slight trend toward reducing the number of unknowns per wavelength as the polynomial degree of the representation increases. (Since these results are obtained with relatively large cells, these figures do not show

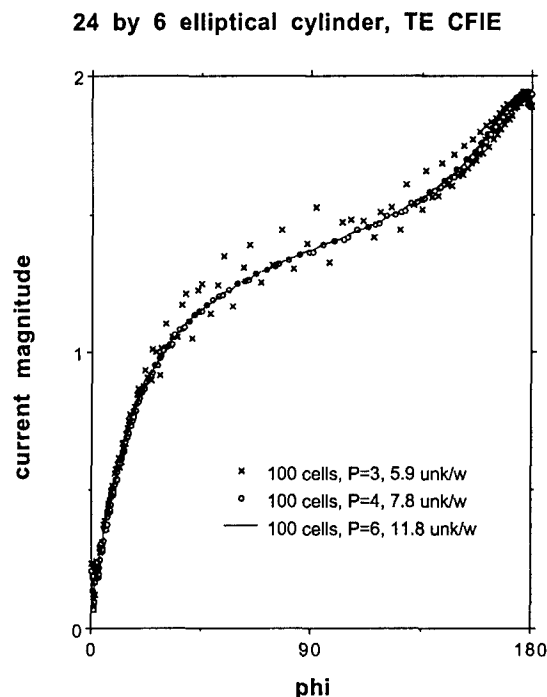the substantial improvement in accuracy possible with higher orders at sufficiently high cell densities.)

24 by 6 elliptical cylinder, TE CFIE

Figure 6. Results from the LCN method using a 100-cell model of an elliptical cylinder of dimensions 24λ by 6λ.

Comment on program complexity

For a fixed degree of representation, an LCN code requires a developmental effort similar to that of an MoM code. Both procedures use MoM-like convolution integrals for the near-diagonal terms. The LCN code also requires samples of the kernel for the off-diagonal terms, an additional routine not required by MoM codes (however, some implementations of MoM codes may use other approximate expressions for widely spaced source and observer points).
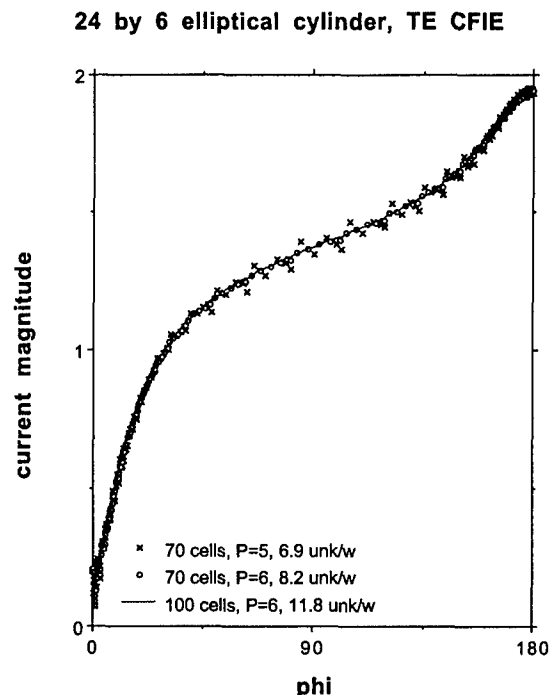
24 by 6 elliptical cylinder, TE CFIE

Figure 7. Results from the LCN method using a 70-cell model of an elliptical cylinder of dimensions 24λ by 6λ.

The primary difference between the LCN and MoM codes is that a P-point LCN implementation essentially includes all the functionality needed to implement lower degrees. By adding the appropriate lower-order quadrature weights and sample points, the LCN code can easily treat degrees from 1 to P. An MoM implementation of degree p does not necessarily include lower degrees. To extend either approach to higher degrees, the programmer must add the additional basis functions, their derivatives, and appropriate procedures to compute the necessary integrals. If numerical quadrature is used to compute the integrals, the extension of either code to other degrees is a relatively straightforward task.

Conclusions

By comparing the accuracy of the current density produced by the MoM and LCN implementations for a number of examples, we arrive at several interesting observations.

First, for the same model and the same number of overlapping functions per cell (MoM) and sample points per cell (LCN), the overall accuracy of the surface current density appears similar. This behavior is observed despite the fact that the LCN representation does not impose cell-to-cell continuity. Because the MoM representation uses one fewer unknown per cell for a given number of overlapping functions, the overall accuracy of the MoM for a given number of unknowns appears to be slightly superior. Both methods produce results that generally appear to follow the expected $O(\Delta^{p+1})$ behavior associated with polynomial interpolation error.

Second, the fact that the LCN can produce accurate results without imposing cell-to-cell continuity suggests that it might be possible to relax continuity conditions in MoM formulations as well. Relaxed continuity conditions may permit the use of non-conformal models that may simplify the meshing procedures for 3D applications (at the cost of slightly more unknowns for a given accuracy).

Third, while the MoM matrix entries are integrals of a particular field, the LCN entries represent samples of the associated integrand, and as such are fundamentally easier to compute in most situations. Thus, the fill time associated with the LCN is usually much faster than that of the MoM for the same equation. Furthermore, the LCN appears to offer advantages for problems where the MoM integrals are especially expensive to compute (one possible example is a multilayer structure where the associated Green's functions typically involve Sommerfeld integrals).

Finally, once a computer program has been developed for a (p+1)-point LCN implementation, it is trivial to extend it to a lower number of points. (Essentially all that is required is including the quadrature rule for the lower orders.) Thus, the LCN offers a relatively easy implementation of p-refinement strategies, where the polynomial degree of the representation can be increased until some measure of accuracy is achieved. Both theory and experience suggest that p-refinement schemes are more efficient than h-refinement schemes (reducing cell sizes to improve accuracy). Adaptive p-refinement techniques, where each cell in a model can have a different order, should also prove easier to program in the context of an LCN approach than in an MoM approach.

References

[1]   R. F. Harrington, *Field Computation by Moment Methods*. New York: IEEE Press, 1993.

[2]   E. J. Nyström, "Über die praktische Auflösung von Integral-gleichungen mit Anwendungen auf Randwertaufgaben," *Acta Math.*, vol. 54, pp. 185-204, 1930.

[3]   K. E. Atkinson, *A Survey of Numerical Methods for the Solution of Fredholm Integral Equations of the Second Kind*. Philadelphia: SIAM, 1976.

[4]   L. F. Canino, J. J. Ottusch, M. A. Stalzer, J. L. Visher, and S. M. Wandzura, "Numerical Solution of the Helmholtz Equation in 2D and 3D Using a High-Order Nyström Discretization," *J. Comp. Physics*, vol. 146, pp. 627-663, 1998.

[5]   G. Liu and S. Gedney, "High-order Nyström solution of the VEFIE for TE-Wave scattering," *Electromagnetics*, vol. 21, No. 1, pp. 1-14, 2001.

[6]   D. R. Wilton and C. M. Butler, "Effective methods for solving integral and integro-differential equations," *Electromagnetics*, vol. 1, pp. 289-308, 1981.

[7] J. H. Ma, V. Rokhlin, and S. Wandzura, "Generalized Gaussian quadrature rules for systems of arbitrary functions," *SIAM J. Numerical Analysis*, vol. 33, pp. 971-996, June 1996.

[8] J. Strain, "Locally corrected multidimensional quadrature rules for singular functions," *SIAM J. Scientific Computing*, vol. 16, pp.992-1017, 1995.

[9] A. F. Peterson, D. R. Wilton, and R. E. Jorgenson, "Variational nature of Galerkin and non-Galerkin moment method solutions," *IEEE Trans. Antennas Propagat.*, vol. 44, pp. 500-503, April 1996.

[10] R. F. Harrington, *Time-harmonic Electromagnetic Fields*. New York: McGraw-Hill, 1961, p. 235.

[11] A. F. Peterson, S. L. Ray, and R. Mittra, *Computational Methods for Electromagnetics*. New York: IEEE Press, 1998, Chapter 6.